Structural basis for TIR domain–mediated innate immune signaling by Toll-like receptor adaptors TRIF and TRAM

Published

2025

Journal Title

Proceedings of the National Academy of Sciences

Version

Version of Record (VoR)

DOI

10.1073/pnas.2418988122

PNAS RESEARCH ARTICLE | IMMUNOLOGY AND INFLAMMATION

Structural basis for TIR domain–mediated innate immune signaling by Toll-like receptor adaptors TRIF and TRAM

Mohammad K. Manik[a,b,1], Mengqi Pan[c,d,e,1], Le Xiao[a,b,1], Weixi Gu[c,d,e,1], Hyoyoung Kim[c,d,1], Sabrina Pospich[f], Andrew Hedger[c,d,e], Parimala R. Vajjhala[c,d], Morris Y. L. Lee[c,d], Xiaoqi Qian[c,d,e], Michael J. Landsberg[c,d,e], Thomas Ve[g], Jeffrey D. Nanson[c,d,e,h], Stefan Raunser[f], Katryn J. Stacey[c,d,e], Hao Wu[a,b,2], and Bostjan Kobe[c,d,e,2]

Affiliations are included on p. 7.

Contributed by Hao Wu; received September 17, 2024; accepted December 10, 2024; reviewed by Pingwei Li and Hyun Ho Park

Innate immunity relies on Toll-like receptors (TLRs) to detect pathogen-associated molecular patterns. The TIR (Toll/interleukin-1 receptor) domain-containing TLR adaptors TRIF (TIR domain–containing adaptor-inducing interferon-β) and TRAM (TRIF-related adaptor molecule) are essential for MyD88-independent TLR signaling. However, the structural basis of TRIF and TRAM TIR domain–based signaling remains unclear. Here, we present cryo-EM structures of filaments formed by TRIF and TRAM TIR domains at resolutions of 3.3 Å and 5.6 Å, respectively. Both structures reveal two-stranded parallel helical arrangements. Functional studies underscore the importance of intrastrand interactions, mediated by the BB-loop, and interstrand interactions in TLR4-mediated signaling. We also report the crystal structure of the monomeric TRAM TIR domain bearing the BB loop mutation C117H, which reveals conformational differences consistent with its inactivity. Our findings suggest a unified signaling mechanism by the TIR domains of the four signaling TLR adaptors MyD88, MAL, TRIF, and TRAM and reveal potential therapeutic targets for immunity-related disorders.

MyD88-independent TLR signaling | TIR domain | cryo-EM | helical reconstruction

Significance

This study elucidates the structural basis of Toll-like receptor (TLR) signaling through the TIR domain–containing adaptor proteins TRIF and TRAM. By using cryoelectron microscopy (cryo-EM) and X-ray crystallography, we provide structural insights into filamentous signaling assemblies formed by TRIF and TRAM TIR domains, shedding light on their molecular architecture and intersubunit interactions, which we validate by mutagenesis and functional assays. These results deepen our understanding of innate immune responses orchestrated by TLR signaling.

The innate immune system serves as the body's first line of defense against microbial pathogens, rapidly detecting and responding to invading threats (1). Central to this defense mechanism are Toll-like receptors (TLRs), a family of transmembrane proteins that recognize conserved microbial molecular patterns (pathogen-associated molecular patterns, PAMPs) (1, 2). Upon ligand binding, TLRs initiate intracellular signaling cascades that activate proinflammatory and antimicrobial responses, essential for host defense and immune regulation (2).

TLR signaling pathways can be broadly categorized into two main branches: the MyD88-dependent pathway and the MyD88-independent pathway. In the former, TLR activation leads to the recruitment of the adaptor protein MyD88 (myeloid differentiation factor 88), and in some cases, the bridging adaptor MAL (MyD88 adaptor-like; also called TIRAP, TIR domain–containing adaptor protein) to the TIR domain of the receptors, initiating downstream signaling events that result in the activation of NF-κB (nuclear factor-kappa B) and MAPKs (mitogen-activated protein kinases), ultimately leading to the production of proinflammatory cytokines (3, 4). Conversely, the MyD88-independent pathway, also known as the TRIF-dependent pathway, engages the alternative adaptor molecules TRIF (TIR-domain-containing adapter-inducing interferon-β, also called TICAM-1, TIR domain–containing adaptor molecule 1), with or without the bridging adaptor TRAM (TRIF-related adaptor molecule, also called TICAM-2), depending on the TLR, to mediate immune responses (5–8). The TRIF-dependent pathway plays a pivotal role in the signaling cascades initiated by TLR3 and TLR4 (9). In response to double-stranded RNA, a typical viral PAMP, TLR3 specifically recruits TRIF, leading to the induction of type I interferons (IFNs) and proinflammatory cytokines (5). TLR4 can signal in response to LPS (lipopolysaccharide) through the adaptors MAL and MyD88 from the cell surface, or through TRAM and TRIF from the endosome (9).

While considerable progress has been made in elucidating the molecular mechanisms underlying TLR signaling and the structural basis of TIR-domain signalosome assembly (see (10, 11) for recent reviews), the structural basis of TIR domain–mediated signaling by TRIF and TRAM, the crucial components of the MyD88-independent pathway, has yet to be characterized. In this study, we employed cryoelectron microscopy (cryo-EM) to investigate the architecture of TRIF and TRAM TIR domain signaling assemblies. Our structures provide insights into their structural organization and conformational dynamics. We validated the interactions observed in these structures by mutagenesis and functional assays.

Author contributions: M.K.M., M.P., L.X., W.G., H.K., A.H., P.R.V., M.Y.L.L., X.Q., M.J.L., T.V., J.D.N., S.R., K.J.S., H.W., and B.K. designed research; M.K.M., M.P., L.X., W.G., H.K., S.P., A.H., P.R.V., M.Y.L.L., X.Q., and J.D.N. performed research; M.K.M., M.P., L.X., W.G., H.K., A.H., J.D.N., K.J.S., and B.K. contributed new reagents/analytic tools; M.K.M., M.P., L.X., W.G., H.K., S.P., A.H., P.R.V., M.Y.L.L., X.Q., M.J.L., T.V., J.D.N., S.R., K.J.S., H.W., and B.K. analyzed data; and M.K.M., M.P., L.X., W.G., H.K., S.P., J.D.N., H.W., and B.K. wrote the paper.

Reviewers: P.L., Texas A&M University; and H.P., Chung-Ang University Faculty of Medicine and Pharmacy.

The authors declare no competing interest.

[1]M.K.M., M.P., L.X., W.G., and H.K. contributed equally to this work.

[2]To whom correspondence may be addressed. Email: wu@crystal.harvard.edu or b.kobe@uq.edu.au.

This article contains supporting information online at https://www.pnas.org/lookup/suppl/doi:10.1073/pnas.2418988122/-/DCSupplemental.

Published January 9, 2025.

Results

TRIF^{TIR} and TRAM^{TIR} Self-Assemble into Filaments. We previously reported the spontaneous self-association of the TIR domain of the adaptor protein MAL (MAL^{TIR}) (12). To assess whether human TRIF^{TIR} and TRAM^{TIR} exhibit similar behavior, we pursued the expression and purification of various TIR-domain constructs from these proteins. For TRIF, we designed mammalian expression constructs that lacked the C-terminal RHIM (receptor-interacting protein [RIP] homotypic interaction motif; TRIF$^{\Delta RHIM}$, residues 1 to 545) or included only the TIR domain (TRIF^{TIR}, residues 387 to 545) (Fig. 1*A*). The expressed proteins were found to be prone to self-association and forming large aggregates, as evidenced by elution in the void volume during purification by Superose 6 size-exclusion chromatography (SEC) (*SI Appendix,* Fig. S1*A*). For TRAM, we designed bacterial expression constructs containing TRAM^{TIR} (residues 70 to 235) and full-length TRAM (TRAM^{FL}, residues 1 to 235). While at lower concentrations (up to ~20 μM) these proteins eluted at a position consistent with a monomeric state during SEC purification (*SI Appendix* Fig. S1*A*), they became viscous at higher concentrations (~120 μM), suggesting the formation of large molecular complexes.

To obtain further insights into these assemblies, we performed negative-stain transmission electron microscopy (EM) analysis of TRIF and TRAM samples. TRIF$^{\Delta RHIM}$-GFP formed filamentous assemblies with a diameter of approximately 15 nm (Fig. 1*B*). Removal of the GFP tag yielded longer filaments of comparable dimensions (Fig. 1*B*). These filaments showed pH-sensitive behavior; negative-stain EM analysis showed that pH 8.0 was optimal for filament formation, whereas pH values below 7.0 had a negative impact (*SI Appendix,* Fig. S1*B*). TRIF^{TIR} formed filaments with and without the presence of GFP; however, removing the C-terminal GFP tag in TRIF^{TIR} caused protein precipitation at higher concentrations. Similarly, negative-stain EM analyses of the viscous solutions of both TRAM^{TIR} and TRAM^{FL} at high concentrations revealed the presence of filaments akin to those observed for TRIF (Fig. 1*B*). These findings support the propensity of TRIF^{TIR} and TRAM^{TIR} to form filaments.

Cryo-EM Structures of TRIF^{TIR} and TRAM^{TIR} Filaments. To obtain structural insights into the mechanism of TRIF^{TIR} and TRAM^{TIR} filament formation, we sought to determine the structures of these assemblies using cryo-EM. For TRIF, we collected cryo-EM data for both TRIF^{TIR} and TRIF$^{\Delta RHIM}$ filaments on a Titan Krios microscope. Filaments were imaged using a pixel size of 0.85 Å at the specimen level, and both 3D reconstructions revealed an identical arrangement of TIR domains (Fig. 1*C*). TRIF$^{\Delta RHIM}$ yielded a higher-resolution cryo-EM map at 3.3 Å (Fig. 1*C* and *SI Appendix* Fig. S2 *A–D* and Table S1). The structure revealed a head-to-tail TIR assembly arranged into two parallel strands with helical symmetry (16.28 Å axial rise and 178.86° helical twist). The TRIF$^{\Delta RHIM}$ cryo-EM density map allowed us to build a model covering amino acids 393-535, which just corresponds to the TIR domain of TRIF (the structure will therefore be referred to as TRIF$^{TIR\text{-}Fil}$; Figs. 1 *A* and *C* and 2*A*). The N-terminal domain preceding residue 393 was not resolved and presumably adopts a dynamic conformation.

For TRAM^{TIR}, the cryo-EM data were collected on a Talos Arctica microscope using a pixel size of 1.7 Å at the specimen level. Data processing was challenging, primarily due to the thick ice in which filaments were predominantly observed, and this complicated the 2D classification process. To solve this problem, we optimized classification parameters and performed two consecutive rounds of 2D classification. This allowed us to rigorously remove contaminants and retain only particles contributing to high-resolution classes. Following extensive optimization, we obtained a 3D reconstruction with a moderate resolution of 5.6 Å, but sufficient to model TRAM amino acids 77 to 231, which corresponds to the TIR domain of TRAM. The structure of TRAM^{TIR} also shows helical symmetry (16.11 Å axial rise and 177.9° helical twist; *SI Appendix,* Fig. S3) and like TRIF$^{TIR\text{-}Fil}$,

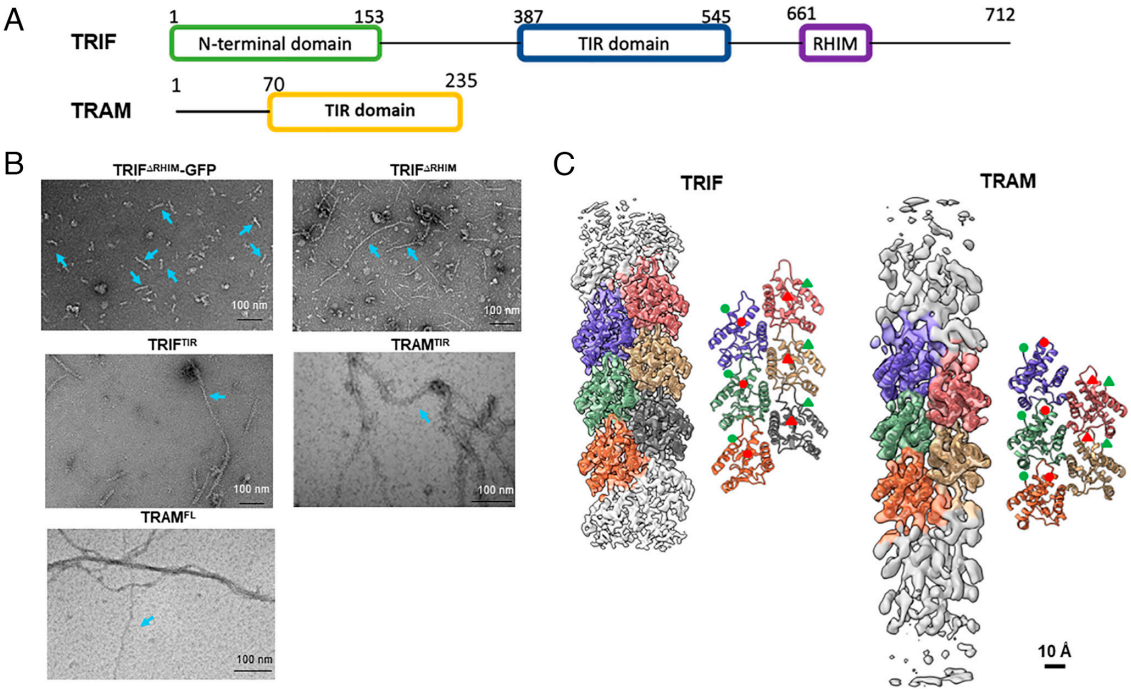

Fig. 1. TRIF and TRAM self-assemble into filaments in vitro. (*A*) Domain architecture of TRIF and TRAM. (*B*) Negative-stain EM analysis for the TRIF$^{\Delta RHIM}$-GFP, TRIF$^{\Delta RHIM}$, TRIF^{TIR}, TRAM^{TIR}, and TRAM^{FL} filaments. Blue arrows indicate filaments. (*C*) Cryo-EM reconstructions of the TRIF$^{\Delta RHIM}$ and TRAM^{TIR} filaments, superimposed with the final atomic models, respectively. The N and C termini are highlighted with green and red circle/triangles, respectively.

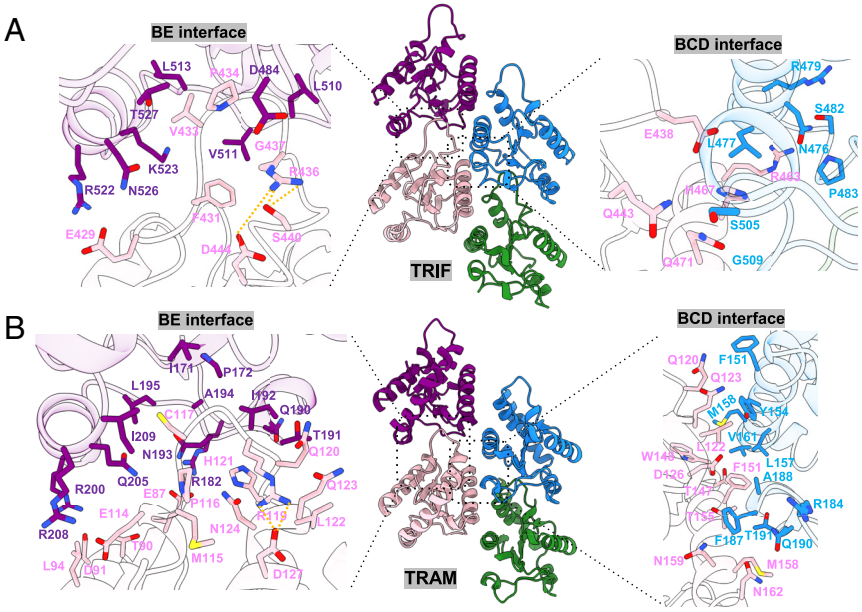

Fig. 2. Cryo-EM structures of TRIF$^{TIR\text{-}Fil}$ and TRAM^{TIR} filaments. (*A*) Two-stranded parallel head-to-tail TRIF$^{TIR\text{-}Fil}$ filamentous assembly is stabilized by the intrastrand BE and the interstrand BCD interfaces. Internal salt bridges are presented as orange dashed lines. (*B*) Two-stranded parallel head-to-tail TRAM^{TIR} filamentous assembly is stabilized by the intrastrand BE and the interstrand BCD interfaces. Internal salt bridges are presented as orange dashed lines.

reveals a filamentous structure composed of two parallel strands of TIR-domain subunits arranged in a head-to-tail configuration (Figs. 1*C* and 2*B* and *SI Appendix,* Fig. S3).

For TRIF$^{TIR\text{-}Fil}$ and TRAM^{TIR} structures, each protomer of the filament shows the canonical TIR structure, consisting of five β-strands (βA-βE) wrapped by five α-helices (αA-αE; the loops are named based on the elements of secondary structure they connect—the BB loop connects strand βB with helix αB; *SI Appendix,* Fig. S4*A*). A superposition of TRIF$^{TIR\text{-}Fil}$ and TRAM^{TIR} structures shows notable differences in the BB loop, αD and αE helices, and βE region (*SI Appendix,* Fig. S4*A*). In addition, TRAM^{TIR} has a more extended αE helix compared to TRIF$^{TIR\text{-}Fil}$.

Two major types of interfaces mediate the formation of TRIF$^{TIR\text{-}Fil}$ and TRAM^{TIR} filaments. The first interface is the head-to-tail intrastrand "BE" interface, with a buried surface area of 1105 Å^2 and 1123 Å^2 for TRIF$^{TIR\text{-}Fil}$ and TRAM^{TIR}, respectively. The intrastrand interface is mediated by hydrophobic interactions involving the BB loop (BB surface) of one TRIF$^{TIR\text{-}Fil}$ protomer interacting with residues of the αE helix and βE strand (EE surface) of the other protomer (Fig. 2*A*). In the TRIF$^{TIR\text{-}Fil}$ filament, the highly conserved proline residue (P434) in the BB loop is buried in a pocket between the βE strand and the αE helix. The interface is stabilized by hydrogen bonds or salt bridges involving the side chains or main chain of interacting residues E429:N526, E429:R522, R436:V511, and R436:D484 (Fig. 2*A*). The internal salt bridges between R436 and D444, as well as hydrogen bonds between R436 and S440 further stabilize the conformation of the BB loop. Although the details of the TRAM^{TIR} model are less reliable due to the lower resolution, the BE interface also appears to be stabilized by several hydrogen bonds and salt bridges, including E87:R182, E114:R208 E114:Q205, and D91:R200 (Fig. 2*B*). TRAM also has a highly conserved proline residue (P116) which is located in the pocket formed by the EE surface (Fig. 2*B*), but unlike TRIF and most other mammalian TLR TIR domains, is not located at the apex of the BB loop. That position is occupied by C117, which is buried in the EE surface hydrophobic pocket. The internal salt bridge between R119 and D127 is also observed in TRAM, where it stabilizes the conformation of the BB loop (Fig. 2*B*).

The second interface is the interstrand "BCD" interface between the two protofilaments, with a buried interface area of 1116 Å^2 and 872 Å^2 for TRIF$^{TIR\text{-}Fil}$ and TRAM^{TIR}, respectively. This interstrand interface is formed by the interactions between the residues from αB, αC, and αD helices (Fig. 2). The TRIF BCD interface involves the side chains and main chain of interacting residues R463:N476, Q471:S505, Q443:S505, R463:S482, R463:L477, R463:R479, R463:P483, and R463:G481 (Fig. 2*A*). The TRAM BCD interface is mainly mediated by the hydrophobic interactions such as L122:Y154, F151:L157, F151:A188, and N162:F187 (Fig. 2*B*).

Structural superpositions of solution NMR structures of the BB-loop mutants TRIF$^{TIR\text{-}P434H}$ (PDB (Protein Data Bank): 2M1X) and TRAM$^{TIR\text{-}C117H}$ (PDB: 2M1W) (13) onto the TRIF$^{TIR\text{-}Fil}$ and TRAM^{TIR} molecules in the respective filaments show substantial conformational differences in the BB-loop region; the BB loop in the solution-structure conformation would clash with the EE surface in the filament (*SI Appendix,* Fig. S4*B*). Assuming that the solution structures of the mutants resemble the structures of wild-type proteins, these observations suggest that conformational changes occur upon filament formation, for both TRIF and TRAM. To gain further insight into these conformational changes, we purified the BB-loop mutant TRAM$^{TIR\text{-}C117H}$. SEC-MALS analysis indicated that the TRAM$^{TIR\text{-}C117H}$ is monomeric in solution over a wide concentration range and negative-stain EM analysis showed no evidence of higher-order assembly for this mutant (*SI Appendix,* Fig. S4*C*). We determined the crystal structure of TRAM$^{TIR\text{-}C117H}$ (*SI Appendix,* Fig. S4*B* and Table S2). The superposition of the solution and crystal structures of TRAM$^{TIR\text{-}C117H}$ shows different orientations of the αC and αE helices and the BB-loop region (*SI Appendix,* Fig. S4*B*). A crystal packing analysis shows two types of interfaces with the buried surface areas of 1482 Å^2 and 573 Å^2; however, neither is found in TRAM^{TIR} filaments or any other characterized TIR-domain assemblies, and thus is not likely to be biologically relevant (*SI Appendix,* Fig. S4*D*). We propose that incorporation of monomers into the filament and the formation of required interfaces involves a rearrangement of the αC and αE helices and the BB-loop region, contributing to the cooperativity of the assembly process.

Comparison of TRAM and TRIF Structures with Those of Other TIR-domains. TRIF$^{TIR\text{-}Fil}$ and TRAM^{TIR} filaments display a two-stranded head-to-tail arrangement, which bears high similarities with the TIR-domain assemblies of MAL and MyD88 characterized previously (12, 14) (Figs. 2 and 3). All these assemblies are held together by analogous interfaces. The individual TIR domains in TRAM and TRIF filaments also show similar conformations to those of MAL (PDB: 5UZB) and MyD88 (PDB: 7BER) in their respective filamentous assemblies (Fig. 3 and *SI Appendix*, Fig. S4*E*). The main differences in structures correspond to the size and positioning of the αE helices, with TRAM^{TIR} featuring an extended αE helix, which is mostly solvent-exposed and largely outside the BE interface. Although minor structural differences are also observed in BB-loop regions, the filamentous structures of all four adaptors display a conformation that extends away from the rest of the domain, different from the conformations observed in the monomeric forms of the respective proteins.

The two-stranded head-to-tail arrangements of TRIF$^{TIR\text{-}Fil}$ and TRAM^{TIR} also share similarities with assemblies formed by bacterial TIR domains, including AbTir (TIR domain–containing protein from *Acinetobacter baumannii*; PDB: 7UXU) and TIR-APAZ (analogue of Piwi–Argonaute–Zwille domain from the SPARTA [short prokaryotic Argonaute TIR-APAZ] complex; PDB: 8IT1), which possess NAD^+-cleavage activity (15, 16) (Fig. 3). Superpositions of these TIR domains revealed a similar 3D structure with conformational differences observed in the BB-loop, αC and αE helix regions (*SI Appendix*, Fig. S4*E*). However, TRIF$^{TIR\text{-}Fil}$ and TRAM^{TIR} are likely unable to cleave NAD^+ due to the lack of the catalytic glutamate in the active site (*SI Appendix*, Fig. S4*A*).

SARM1 (sterile alpha and Toll/interleukin-1 receptor motif-containing 1) is a TIR domain–containing adaptor protein down-regulating TRIF-dependent TLR signaling via directly targeting TRIF (17). However, its main role is to degrade NAD^+ in neurons, to promote axon degeneration upon physical injury, neuroinflammation, and toxic or metabolic disorders (18). Upon activation, the TIR domain of SARM1 assembles into a similar head-to-tail arrangement seen in both TRIF$^{TIR\text{-}Fil}$ and TRAM^{TIR} filaments. In SARM1, however, the two strands are packed in an antiparallel, rather than parallel manner (Fig. 3). Thus, the interstrand BCD interface in TRIF$^{TIR\text{-}Fil}$ and TRAM^{TIR} filaments is not observed in SARM1 filaments. Instead, SARM1 uses an alternative "AE" interface to stabilize the interstrand interaction. Structural comparison of the TIR domains from TRAM and TRIF filaments with SARM1^{TIR} (PDB: 7NAK), shows major differences in the CC-loop and αD and αE helix regions (Fig. 3, *SI Appendix*, Fig. S4*E*). SARM1 has an extended CC-loop and αD helix, which likely prevents the recruitment of other TIR subunits to the BCD interface, and therefore uses an alternative interstrand AE interface instead. This different TIR arrangement seen in TRIF$^{TIR\text{-}Fil}$ and SARM1^{TIR} filaments may also explain why SARM1 is able to inhibit the TRIF-dependent signaling – if SARM1 is recruited by TRIF via the BE interface, it would terminate signaling, by being unable to form the BCD interface. The antiparallel two-stranded arrangement of TIR domains is also observed for plant TIR domains (19, 20) (Fig. 3).

Mutations of TRAM^{TIR} Residues Involved in Intrastrand and Interstrand Interfaces Disrupt Signaling. To probe the functional significance of specific residues within the intrastrand and interstrand interfaces of TRAM^{TIR}, we performed site-directed mutagenesis and tested the effects of mutations on filament assembly and cell signaling. To develop a reporter system for TRAM/TRIF-mediated signaling, we tested an IRF3 (interferon-regulatory factor 3)-dependent reporter (21) in TLR4/MD2 (myeloid differentiation factor 2)/CD14 (cluster of differentiation 14)-expressing HEK293 (human embryonic kidney) cells, but found the IRF3-driven reporter had very little response to LPS treatment. This is consistent with the finding that adenoviral protein E1A, which is expressed in HEK293 cells, suppresses TBK1-mediated IRF3 phosphorylation (22). Given that the TRIF pathway also activates NF-κB (23–25), we utilized HEK293 cells expressing TLR4/MD2/CD14 with an integrated NF-κB-driven mScarlet-I reporter gene and the *MYD88* gene knocked out (here termed MYD88 KO reporter cells), to assess TRAM/TRIF-mediated signaling (26). We found that the expression level

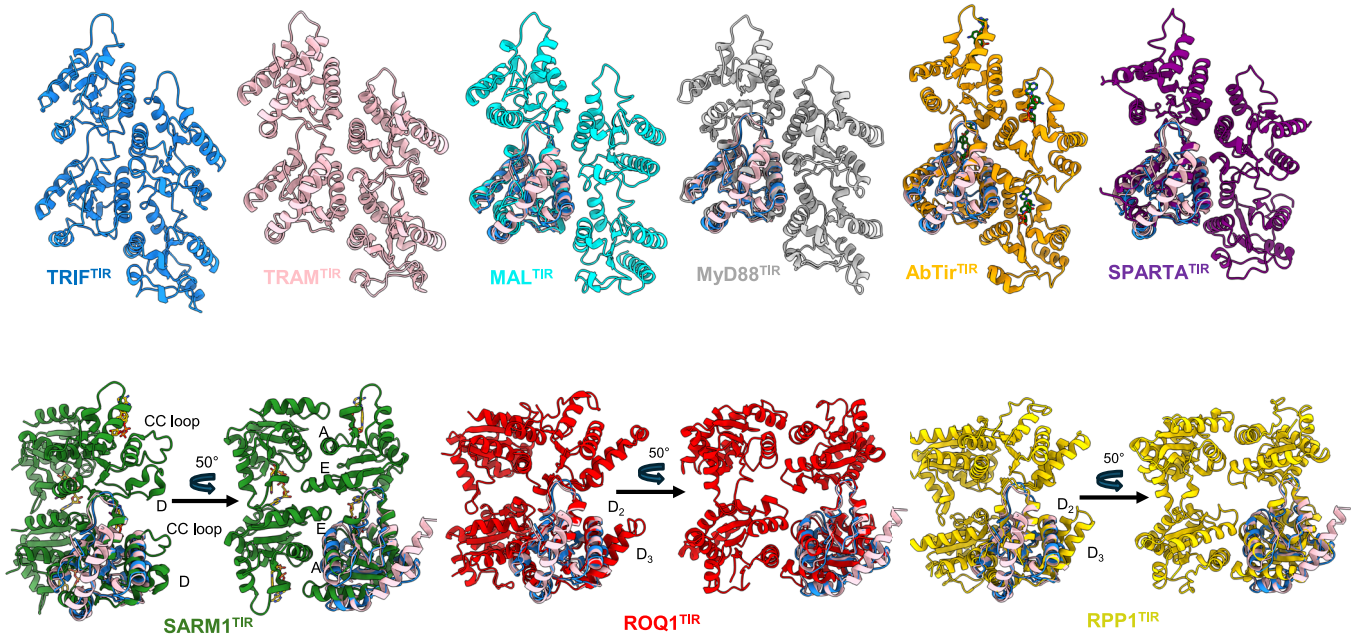

Fig. 3. Structural superposition of individual subunits of TRIF$^{TIR\text{-}Fil}$ (blue) and TRAM^{TIR} (pink) from the respective filaments onto the two-stranded parallel filamentous assemblies (*Top* row) of MAL (cyan, PDB: 5UZB), MyD88 (gray, PDB: 7BEQ), AbTir (orange, PDB: 7UXU), and SPARTA (purple, PDB: 8IT1) and two-stranded antiparallel filamentous assemblies (*Bottom* row) of SARM1 (green, PDB: 7NAK), ROQ1 (red, PDB: 7JLX), and RPP1 (yellow, PDB: 7DFV).

of endogenous TRAM in these cells was insufficient to trigger MyD88-independent NF-κB activation via TRIF signaling (*SI Appendix,* Fig. S5 *A* and *B*). However, the cells gained LPS responsiveness with exogenous TRAM expression (*SI Appendix,* Fig. S5*A*). Thus, these cells permit assessment of the effects of TRAM variants on TLR4 signaling activity.

We previously showed the benefit of using a dual-fluorophore flow cytometric assay to simultaneously follow the level of NF-κB-driven signaling activity with mScarlet and the level of the signaling protein of interest tagged with GFP (26). By flow cytometry, we can select to analyze only the cells that express TRAM-GFP at modest levels, excluding both untransfected cells and constitutively active populations expressing high levels of TRAM-GFP (*SI Appendix,* Fig. S5*A*). The overall expression of all the mutants, except for Q190A, L195A, and W148A, was similar to the wild-type (WT) protein, although even Q190A, L195A, and W148A showed adequate expression within the analysis gate (*SI Appendix,* Fig. S6). We tested TRAM mutants in both the intrastrand and interstrand interfaces, and most had profound effects on signaling—either decreasing or increasing activity (Fig. 4). Substitution of the charged residues in the TRAM head-to-tail interface (E87A, R182A, E114R, R208E, and R119E, but not D91A and R200A) abolished NF-κB activation, suggesting the importance of E87:R182 and E114:R208 electrostatic interactions in the head-to-tail interface, as well as the internal R119:D128 salt bridge in stabilizing the BB loop. Furthermore, the inactive C117H mutant is consistent with the residue's location in the hydrophobic pocket formed by I171, L195, I209, and F210 in the EE surface. In the interstrand interfaces, mutations of nonpolar residues (L122A, W148A, F151A, L157S, M158R, and F187A) decreased

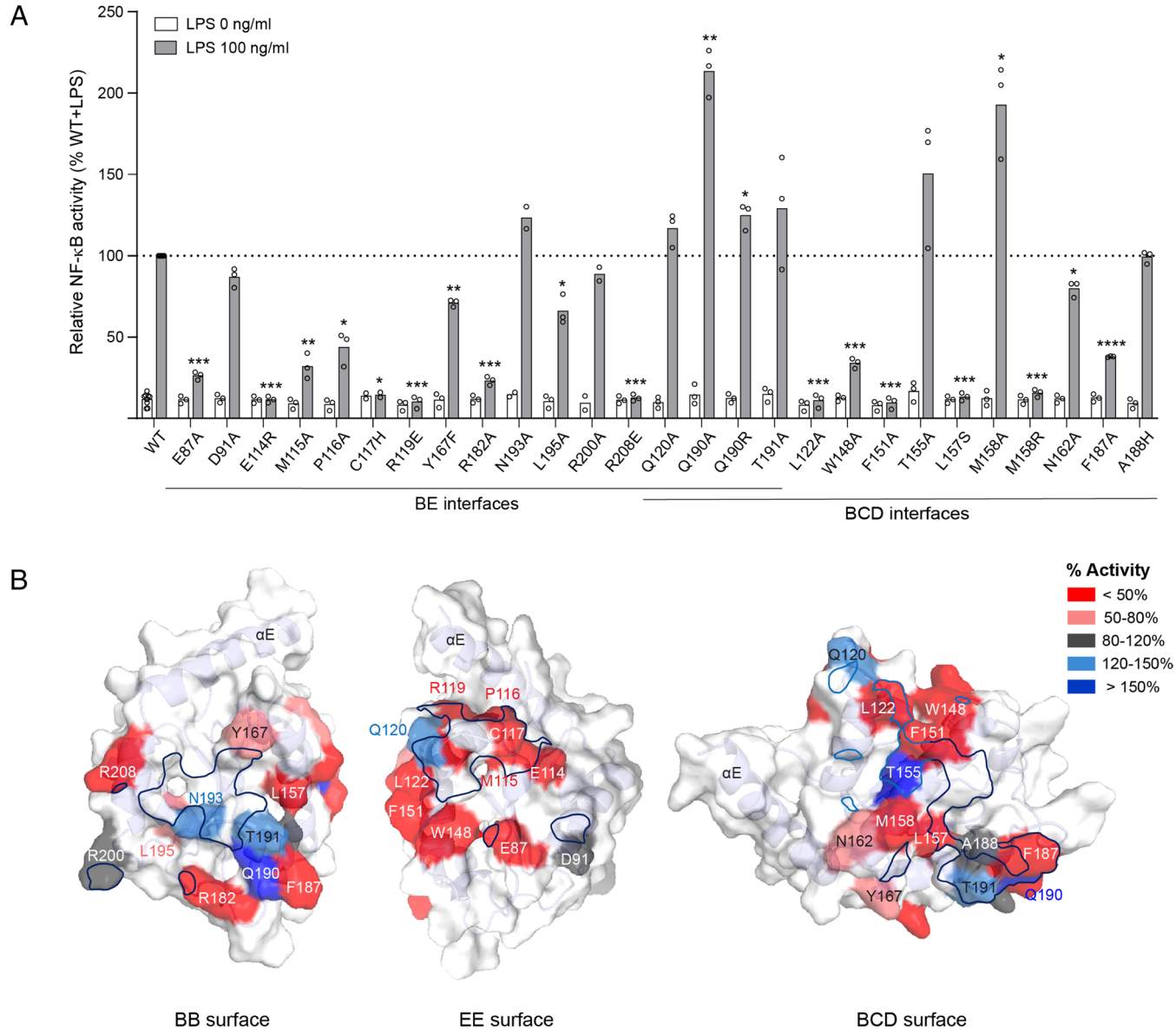

Fig. 4. Analysis of effects of mutations of residues in the TRAM:TRAM interaction interfaces on signaling efficiency. (*A*) MyD88 KO reporter cells were transiently transfected with 100 ng TRAM-GFP constructs (WT or mutants). On the following day, the cells were treated with or without 100 ng/ml LPS and incubated for 16 h. The cells were harvested and run on a flow cytometer. Cells expressing TRAM-GFP at a modest level were selected for analysis (*SI Appendix,* Fig. S5*A*). NF-κB-driven mScarlet-I reporter expression for each mutant was normalized to LPS-stimulated WT control (% WT + LPS). Results are from 2 to 3 independent experiments. Each dot indicates the mean of duplicates within an individual experiment. Note that WT controls were done 9 times, as they were included for every single experiment. ****$P < 0.0001$, ***$P < 0.001$, **$P < 0.01$, or *$P < 0.05$ compared to WT + LPS in one sample *t* test. (*B*) All the mutated residues are mapped on the $TRAM^{TIR}$ structure and highlighted according to their effect on the signaling. The blue lines represent the physical contact area between TRAMs (identified by using the PyMOL software); for BCD interfaces, the interactions with two molecules are shown by two different shades of blue. Note that the effects of Q190A and M158R were chosen for those residues as more than one mutant was tested.

signaling activities by more than 50% compared to the WT protein, but changes to polar residues (Q120A and N162A) had little effect. These observations suggest that hydrophobic interactions are dominant in the interstrand interaction. In addition, the alanine mutations of Q190, a residue that participates in both interfaces, and M158, a residue that participates in the interstrand interface, doubled the NF-κB activity upon LPS stimulation. These residues are both highly conserved with variants restricted in evolution to arginine or bulky hydrophobic residues respectively, suggesting that restraint of signaling by these residues is important to avoid adverse hyperinflammation.

Commensurate with the results of the functional assays, negative-stain EM experiments show that the P116A, C117H, L125A, and R208E mutations in the intrastrand interface, and the L122A, F151A, and L157S mutations in the interstrand interface, all abolish TRAM filament formation (*SI Appendix,* Figs. S4*C* and S5*C*). Jointly, our mutational analyses underscore the pivotal roles of both intrastrand and interstrand interfaces within the TRAM TIR domain in orchestrating the activation of the TLR4 signaling pathway.

Discussion

TRIF is a key adaptor protein mediating TLR3 and TLR4-associated innate immune signaling. TRIF, as well as its bridging adaptor protein TRAM, spontaneously form filamentous assemblies in vitro, mirroring the behaviors seen for the TIR domains of MyD88 and MAL, the key adaptor proteins regulating the MyD88-dependent TLR signaling pathways. The similar arrangement of head-to-tail TIR domains packed into two parallel strands observed for all these adaptor proteins indicates a conserved structural mechanism governing signal transduction in both MyD88- and TRIF-dependent TLR signaling pathways.

TRIF contains three main structural regions, the NTD (N-terminal domain), the TIR domain, and the RHIM (Fig. 1*A*). In the resting state, the TRIF NTD interacts with the central TIR domain, likely interfering with protein self-association through TIR:TIR and RHIM:RHIM interactions, and the subsequent association with downstream signaling molecules that leads to the activation of transcription factors IRF-3 and NF-κB (27–29). Although we included the NTD in the TRIF protein that we used for cryo-EM studies, we were unable to observe any density for the NTD in our cryo-EM density map, suggesting that the N-terminal portion of TRIF (the NTD and the linker between the NTD and the TIR domain, residues 1 to 387) is not ordered relative to the TIR-domain filament. Release of the TIR domain from the NTD through the binding of TLR3 or TRAM TIR domains presumably permits self-association into the parallel two-stranded head-to-tail filamentous assembly. A number of cell-based mutagenesis studies of the TIR domains of the adaptor proteins MAL (12), MyD88 (14), and TRAM (this study), and of TLRs such as TLR2 (30) and TLR3 (5), demonstrate the importance of the intrastrand BE and interstrand BCD interfaces on signaling in cells. These observations confirm that the filamentous assemblies of TIR domains of TRIF and TRAM, determined in this study, reflect the key protein:protein interactions responsible for signal transduction in cells upon the activation of TLR signaling.

In humans, TLR4 is unique among the TLRs due to the dual recruitment of either MyD88 (with MAL as a bridging adaptor) or TRIF (with TRAM as a bridging adaptor), depending on its localization in cells. In the plasma membrane, TLR4 recruits MAL and subsequently MyD88 to initiate signaling, while in the endosomal membrane, TLR4 utilizes TRAM and TRIF to engage the downstream pathway (7, 31). The assemblies of TIR domains in these adaptor proteins are similar, suggesting that the recruitment mechanisms used by TLR4 are likely similar. However, MAL is preferentially recruited to the PIP2 (phosphatidylinositol 4,5-bisphosphate)-enriched plasma membrane, due to its PIP2-binding motif at the N terminus (residues 15 to 35) (32, 33). On the other hand, TRAM is trafficked from the cell membrane to the endosomal compartment, but independently from TLR4/CD14; this localization depends on its myristoylation motif that facilitates its anchoring to the endosomal membrane (34, 35). This differential localization of the adaptors may explain the specific recruitment of different sets of adaptor proteins to the same receptor.

TLR3 is the other TLR that specifically recruits TRIF to signal, without the assistance of TRAM (6). Despite the similar assemblies formed by the TIR domains of TRIF and TRAM, the surface electrostatic potentials of these TIR domains are slightly different, potentially playing a role in the exclusive recruitment of TRIF in TLR3 signaling (*SI Appendix,* Fig. S1*C*).

The recruitment of adaptor proteins in TLR signaling is a complex process, with posttranslational modifications playing a key role. Ligand-dependent phosphorylation of Tyr759 (βA strand) and Tyr858 (αD helix) of TLR3 by protein tyrosine kinases such as EGFR (epidermal growth factor receptor), Src and Bruton's tyrosine kinase, is required for TRIF recruitment to initiate TLR3 signaling (36, 37). K27-linked polyubiquitination of the TRIF residue Lys523 (αE helix), mediated by the cullin-3-Rbx1-KCTD10 E3 ubiquitin ligase complex, is responsible for the initiation of TLR3 and TLR4 signaling pathways at early time-points (~10 to 15 min), while USP19-mediated deubiquitination of TRIF at later time-points (after ~40 to 60 min) leads to the termination of both signaling responses (38). Notably, the residues modified by posttranslational modifications are mainly present in either the BE or BCD functionally important interfaces observed in our filamentous structures.

SARM1 is the only TLR adaptor protein found to possess NADase activity (39) and has been reported to negatively regulate TRIF-dependent signaling when overexpressed (17). We speculate that negative regulation could result from $SARM1^{TIR}$ being incorporated into growing TRIF filaments via the BE interface head-to-tail interactions, but being unable to form the BCD interface, and thus halting signalosome formation. Like SARM1, many bacterial TIR domains have been shown to have NADase activity, particularly those involved in antiphage defense (40). While TRIF, TRAM, MAL, and MyD88 TIR domains form higher-order assemblies similar to the enzymatically active AbTir and SPARTA TIR domains, none of these human adaptor proteins contains the equivalent of the catalytic glutamate conserved in TIR NADases, consistent with their lack of catalytic activity.

TRAM and TRIF TIR domains share some structural similarities with the bacterial TIR-STING (TIR domain fused to the STING [stimulator of interferon genes] domain) (41). The C-terminal region of TRIF has been reported to interact with and stabilize human STING (42). TRIF has also been reported to from complexes with RNA helicases DDX1, DDX21, and DHX36, to sense dsRNA in dendritic cells (43). Recently, some plant TIR domain–containing proteins have been shown to bind and cleave DNA and RNA and in turn produce signaling molecules (44). Filamentous structures of TRIF and TRAM TIR domains feature different TIR:TIR interfaces compared to the DNA-bound plant TIR domains, but so do the TIR domains within plant resistosome complexes. It remains to be seen whether TRIF (or mammalian TIR domains in general) can function as innate-immunity sensors of cytoplasmic DNA, like STING and AIM2 (absent in melanoma 2), for example (45).

In conclusion, the structures of TRIF and TRAM TIR-domain signalosomes support signaling mechanisms analogous to those proposed for the adaptors MAL and MyD88 and the corresponding higher-order assembly signaling or SCAF (signaling by

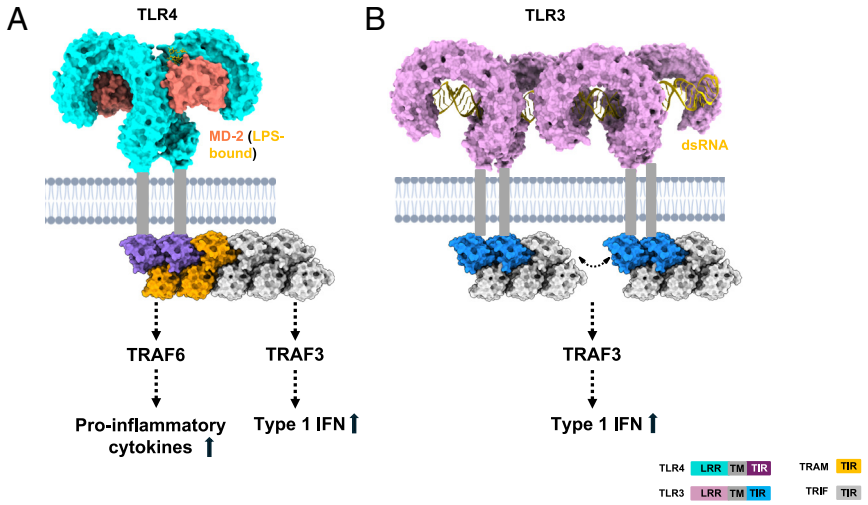

Fig. 5. Schematic diagrams of the mechanisms of signaling by (*A*) TLR4 and the adaptors TRAM and TRIF and (*B*) TLR3 and the adaptor TRIF. Only the TIR domains of the adaptors are shown (TLR4^{TIR}: purple (AlphaFold two-predicted model); TLR3^{TIR}: blue (AlphaFold 2-predicted model); TRIF$^{TIR\text{-}Fil}$: gray; TRAM^{TIR}: orange). Dimerized TLR TIR domains serve as templates to recruit the adaptor proteins through structurally analogous filamentous assemblies and initiate downstream signaling. TRAF3/6: tumor necrosis factor receptor-associated factor 3/6; IFN: interferon.

cooperative assembly formation) models of signal transduction (46–49) (Fig. 5). Building on the models proposed for MAL and MyD88 TIR domains (11, 12, 14), in the case of TLR4, the dimerization of its TIR domain upon LPS recognition would nucleate a filamentous assembly of TRAM TIR domains, which in turn would serve as a template to initiate a structurally analogous filamentous assembly of TRIF TIR domains. Conceptually comparable to the association of MyD88 TIR domains triggering the helical assembly of MyD88 death domains and the recruitment of IRAKs (interleukin-1 receptor associated kinases) (50), in the case of TRIF, TIR domain association would in turn increase the local concentration of TRIF RHIMs and trigger their recruitment of RHIM-containing kinases RIP1 and RIP3, leading to NF-κB activation and cell death (8, 51). In the case of TLR3, the dimerization of its TIR domains would nucleate the assembly of TRIF TIR domains directly; similarly, most TLR TIR domains presumably recruit MyD88 TIR domains directly, as recently characterized in vitro for TLR2 TIR domains (52). Future studies focusing on elucidating the regulation of TLR signaling components hold promise for advancing our understanding of immune system modulation and the development of targeted therapeutics for immunity-related disorders.

Methods

Details of the methods used are provided in *SI Appendix*, Supporting text: Methods, including protein production and purification, cryoelectron microscopy of the TRIF$^{\Delta RHIM}$ and TRAM^{TIR} filaments, crystal structure determination of TRAM$^{TIR\text{-}C117H}$, site-directed mutagenesis, flow cytometry, isolation of human monocyte-derived macrophages, and quantitative reverse transcription PCR (RT-qPCR).

Data, Materials, and Software Availability. All study data are included in the article and/or supporting information. The atomic coordinates and cryo-EM map have been deposited in the Protein Data Bank (PDB), http://www.rcsb.org/ (PDB ID codes 9DK8 (53), 9DKI (54), and 9DLG (55)), and the EM Data Resource, https://www.emdataresource.org/ (ID codes EMD-46946 (56) and EMD-46977 (57)).

ACKNOWLEDGMENTS. We acknowledge the use of the Australian Synchrotron MX facility and thank the staff; the University of Queensland (UQ) Centre for Microscopy and Microanalysis including the UQ-ROCX (Remote Operation Crystallization and X-ray Diffraction) Facility and thank the staff; the University of Melbourne Bio21 Institute Cryo-EM facility and thank the staff; the Harvard Cryo-Electron Microscopy Center for Structural Biology (HC^{2}EM); and the SBgrid Consortium for data processing computer support. This research was funded by the National Health and Medical Research Council (NHMRC Australia; Investigator Grant 1196590 to T.V.; Investigator Grant 2025931 to B.K.); Australian Research Council (ARC) Future Fellowship FT200100572 to T.V., Laureate Fellowship FL180100109 to B.K. and DECRA DE170100783 to T.V.; the US National Institutes of Health (R37AI050872 to H.W.); and the Max Planck Society (to S.R.). MKM was supported by the CRI Irvington Research Fellowship.

Author affiliations: [a]Department of Biological Chemistry and Molecular Pharmacology, Harvard Medical School, Boston, MA 02115; [b]Program in Cellular and Molecular Medicine, Boston Children's Hospital, Boston, MA 02115; [c]School of Chemistry and Molecular Biosciences, University of Queensland, Brisbane, QLD 4072, Australia; [d]Australian Infectious Diseases Research Centre, University of Queensland, Brisbane, QLD 4072, Australia; [e]Institute for Molecular Bioscience, University of Queensland, Brisbane, QLD 4072, Australia; [f]Department of Structural Biochemistry, Max Planck Institute of Molecular Physiology, Dortmund 44227, Germany; [g]Institute for Biomedicine and Glycomics, Griffith University, Gold Coast, QLD 4215, Australia; and [h]Gulbali Institute, Charles Sturt University, Wagga Wagga, NSW 2678, Australia

1. R. Medzhitov *et al.*, Innate immunity. *N. Engl. J. Med.* **343**, 338–344 (2000).
2. S. Akira *et al.*, Pathogen recognition and innate immunity. *Cell* **124**, 783–801 (2006).
3. R. Ferrao *et al.*, IRAK4 dimerization and trans-autophosphorylation are induced by Myddosome assembly. *Mol. Cell* **55**, 891–903 (2014).
4. S. C. Lin *et al.*, Helical assembly in the MyD88-IRAK4-IRAK2 complex in TLR/IL-1R signalling. *Nature* **465**, 885–890 (2010).
5. H. Oshiumi *et al.*, TICAM-1, an adaptor molecule that participates in Toll-like receptor 3-mediated interferon-beta induction. *Nat. Immunol.* **4**, 161–167 (2003).
6. H. Oshiumi *et al.*, TIR-containing adapter molecule (TICAM)-2, a bridging adapter recruiting to Toll-like receptor 4 TICAM-1 that induces interferon-beta. *J. Biol. Chem.* **278**, 49751–49762 (2003).
7. M. Yamamoto *et al.*, TRAM is specifically involved in the Toll-like receptor 4-mediated MyD88-independent signaling pathway. *Nat. Immunol.* **4**, 1144–1150 (2003).
8. M. O. Ullah *et al.*, TRIF-dependent TLR signaling, its functions in host defense and inflammation, and its potential as a therapeutic target. *J. Leukoc Biol.* **100**, 27–45 (2016).
9. K. A. Fitzgerald *et al.*, LPS-TLR4 signaling to IRF-3/7 and NF-kappaB involves the Toll adapters TRAM and TRIF. *J. Exp. Med.* **198**, 1043–1055 (2003).
10. S. Nimma *et al.*, Structural evolution of TIR-domain signalosomes. *Front Immunol.* **12**, 784484 (2021).
11. A. Bhatt *et al.*, Structural characterization of TIR-domain signalosomes through a combination of structural biology approaches. *IUCrJ* **11**, 695–707 (2024).
12. T. Ve *et al.*, Structural basis of TIR-domain-assembly formation in MAL- and MyD88-dependent TLR4 signaling. *Nat. Struct. Mol. Biol.* **24**, 743–751 (2017).
13. Y. Enokizono *et al.*, Structures and interface mapping of the TIR domain-containing adaptor molecules involved in interferon signaling. *Proc. Natl. Acad. Sci. U.S.A.* **110**, 19908–19913 (2013).
14. M. T. B. Clabbers *et al.*, MyD88 TIR domain higher-order assembly interactions revealed by microcrystal electron diffraction and serial femtosecond crystallography. *Nat. Commun.* **12**, 2578 (2021).
15. X. Gao *et al.*, Nucleic-acid-triggered NADase activation of a short prokaryotic Argonaute. *Nature* **625**, 822–831 (2024).

16. M. K. Manik *et al.*, Cyclic ADP ribose isomers: Production, chemical structures, and immune signaling. *Science* **377**, eadc8969 (2022).
17. M. Carty *et al.*, The human adaptor SARM negatively regulates adaptor protein TRIF-dependent Toll-like receptor signaling. *Nat. Immunol.* **7**, 1074–1081 (2006).
18. E. L. Hopkins *et al.*, A novel NAD signaling mechanism in axon degeneration and its relationship to innate immunity. *Front Mol. Biosci.* **8**, 703532 (2021).
19. R. Martin *et al.*, Structure of the activated ROQ1 resistosome directly recognizing the pathogen effector XopQ. *Science* **370**, eabd9993 (2020).
20. S. Ma *et al.*, Direct pathogen-induced assembly of an NLR immune receptor complex to form a holoenzyme. *Science* **370**, eabe3069 (2020).
21. T. Fujita *et al.*, Interferon-beta gene regulation: tandemly repeated sequences of a synthetic 6 bp oligomer function as a virus-inducible enhancer. *Cell* **49**, 357–367 (1987).
22. K. Burleigh *et al.*, Human DNA-PK activates a STING-independent DNA sensing pathway. *Sci. Immunol.* **5**, eaba4219 (2020).
23. K. J. Han *et al.*, Mechanisms of the TRIF-induced interferon-stimulated response element and NF-kappaB activation and apoptosis pathways. *J. Biol. Chem.* **279**, 15652–15661 (2004).
24. K. Hoebe *et al.*, Identification of Lps2 as a key transducer of MyD88-independent TIR signalling. *Nature* **424**, 743–748 (2003).
25. M. Sasai *et al.*, Direct binding of TRAF2 and TRAF6 to TICAM-1/TRIF adaptor participates in activation of the Toll-like receptor 3/4 pathway. *Mol. Immunol.* **47**, 1283–1291 (2010).
26. T. W. Muusse *et al.*, Flow cytometric reporter assays provide robust functional analysis of signaling complexes. *J. Biol. Chem.* **298**, 102666 (2022).
27. M. Tatematsu *et al.*, A molecular mechanism for Toll-IL-1 receptor domain-containing adaptor molecule-1-mediated IRF-3 activation. *J. Biol. Chem.* **285**, 20128–20136 (2010).
28. K. Funami *et al.*, Homo-oligomerization is essential for Toll/interleukin-1 receptor domain-containing adaptor molecule-1-mediated NF-kappaB and interferon regulatory factor-3 activation. *J. Biol. Chem.* **283**, 18283–18291 (2008).
29. M. O. Ullah *et al.*, The TLR signalling adaptor TRIF/TICAM-1 has an N-terminal helical domain with structural similarity to IFIT proteins. *Acta Crystallogr. D Biol. Crystallogr.* **69**, 2420–2430 (2013).
30. J. K. Gautam *et al.*, Structural and functional evidence for the role of the TLR2 DD loop in TLR1/TLR2 heterodimerization and signaling. *J. Biol. Chem.* **281**, 30132–30142 (2006).
31. L. A. O'Neill *et al.*, The family of five: TIR-domain-containing adaptors in Toll-like receptor signalling. *Nat. Rev. Immunol.* **7**, 353–364 (2007).
32. K. S. Bonham *et al.*, A promiscuous lipid-binding protein diversifies the subcellular sites of Toll-like receptor signal transduction. *Cell* **156**, 705–716 (2014).
33. J. C. Kagan *et al.*, Phosphoinositide-mediated adaptor recruitment controls Toll-like receptor signaling. *Cell* **125**, 943–955 (2006).
34. J. C. Kagan *et al.*, TRAM couples endocytosis of Toll-like receptor 4 to the induction of interferon-beta. *Nat. Immunol.* **9**, 361–368 (2008).
35. D. C. Klein *et al.*, CD14, TLR4 and TRAM show different trafficking dynamics during LPS stimulation. *Traffic* **16**, 677–690 (2015).
36. M. Yamashita *et al.*, Epidermal growth factor receptor is essential for Toll-like receptor 3 signaling. *Sci. Signal* **5**, ra50 (2012).
37. K. G. Lee *et al.*, Bruton's tyrosine kinase phosphorylates Toll-like receptor 3 to initiate antiviral response. *Proc. Natl. Acad. Sci. U.S.A.* **109**, 5791–5796 (2012).
38. X. Wu *et al.*, Regulation of TRIF-mediated innate immune response by K27-linked polyubiquitination and deubiquitination. *Nat. Commun.* **10**, 4115 (2019).
39. K. Essuman *et al.*, Shared TIR enzymatic functions regulate cell death and immunity across the tree of life. *Science* **377**, eabo0001 (2022).
40. S. Li *et al.*, Toll/interleukin-1 receptor domains in bacterial and plant immunity. *Curr. Opin. Microbiol.* **74**, 102316 (2023).
41. B. R. Morehouse *et al.*, Cryo-EM structure of an active bacterial TIR-STING filament complex. *Nature* **608**, 803–807 (2022).
42. X. Wang *et al.*, STING requires the adaptor TRIF to trigger innate immune responses to microbial infection. *Cell Host Microbe.* **20**, 329–341 (2016).
43. Z. Zhang *et al.*, DDX1, DDX21, and DHX36 helicases form a complex with the adaptor molecule TRIF to sense dsRNA in dendritic cells. *Immunity* **34**, 866–878 (2011).
44. D. Yu *et al.*, TIR domains of plant immune receptors are 2′,3′-cAMP/cGMP synthetases mediating cell death. *Cell* **185**, 2370–2386.e18 (2022).
45. B. Briard *et al.*, DNA sensing in the innate immune response. *Physiology* **35**, 112–124 (2020).
46. H. Wu, Higher-order assemblies in a new paradigm of signal transduction. *Cell* **153**, 287–292 (2013).
47. P. R. Vajjhala *et al.*, The molecular mechanisms of signaling by cooperative assembly formation in innate immunity pathways. *Mol. Immunol.* **86**, 23–37 (2017).
48. A. Rodriguez Gama *et al.*, Mechanics of a molecular mousetrap-nucleation-limited innate immune signaling. *Biophys. J.* **120**, 1150–1160 (2021).
49. J. C. Kagan *et al.*, SMOCs: supramolecular organizing centres that control innate immunity. *Nat. Rev. Immunol.* **14**, 821–826 (2014).
50. S. C. Lin *et al.*, Helical assembly in the MyD88–IRAK4–IRAK2 complex in TLR/IL-1R signalling. *Nature* **465**, 885–890 (2010).
51. E. Meylan *et al.*, RIP1 is an essential mediator of Toll-like receptor 3-induced NF-kappa B activation. *Nat. Immunol.* **5**, 503–507 (2004).
52. Y. Li *et al.*, Microcrystal electron diffraction structure of Toll-like receptor 2 TIR-domain-nucleated MyD88 TIR-domain higher-order assembly. *Acta Crystallogr. Sect. D* **80**, 699–712 (2024).
53. M. K. Manik, L. Xiao, H. Wu, TRIF TIR filament cryo-EM structure. Protein Data Bank. https://www.rcsb.org/structure/unreleased/9DK8. Deposited 8 September 2024.
54. M. Pan, W. Gu, J. D. Nanson, B. Kobe, Crystal structure of the TIR domain C117H mutant from human TRAM. Protein Data Bank. https://www.rcsb.org/structure/9DKI. Deposited 9 September 2024.
55. A. Hedger *et al.*, CryoEM structure of the TIR domain from human TRAM. Protein Data Bank. https://www.rcsb.org/structure/9DLG. Deposited 11 September 2024.
56. M. K. Manik, L. Xiao, H. Wu, TRIF TIR filament cryo-EM structure. Electron Microscopy Data Bank. https://www.emdataresource.org/EMD-46946. Deposited 8 September 2024.
57. A. Hedger *et al.*, CryoEM structure of the TIR domain from human TRAM. Electron Microscopy Data Bank. https://www.emdataresource.org/EMD-46977. Deposited 11 September 2024.